The Astronomical Journal, 151:69 (12pp), 2016 March doi:10.3847/0004-6256/151/3/69

ASAS J083241+2332.4: A NEW EXTREME LOW MASS RATIO OVERCONTACT BINARY SYSTEM

K. Sriram[1,2], S. Malu[1], C. S. Choi[2], and P. Vivekananda Rao[1]
[1] Department of Astronomy, Osmania University, Hyderabad 500007, India; astrosriram@yahoo.co.in
[2] Korea Astronomy and Space Science Institute, Daejeon 34055, Korea
Received 2015 July 20; accepted 2015 December 28; published 2016 February 23

ABSTRACT

We present the R- and V-band CCD photometry and Hα line studies of an overcontact binary ASAS J083241+2332.4. The light curves exhibit totality along with a trace of the O'Connell effect. The photometric solution indicates that this system falls into the category of extreme low-mass ratio overcontact binaries with a mass ratio, $q \sim 0.06$. Although a trace of the O' Connell effect is observed, constancy of the Hα line along various phases suggest that a relatively higher magnetic activity is needed for it to show a prominent fill-in effect. The study of O–C variations reveals that the period of the binary shows a secular increase at the rate of $dP/dt \sim 0.0765$ s years^{-1}, which is superimposed by a low, but significant, sinusoidal modulation with a period of ~8.25 years. Assuming that the sinusoidal variation is due to the presence of a third body, orbital elements have been derived. There exist three other similar systems, SX Crv, V857 Her, and E53, which have extremely low mass ratios and we conclude that ASAS J083241+2332.4 resembles SX Crv in many respects. Theoretical studies indicate that at a critical mass ratio range, $q_{\rm critical} = 0.07$–0.09, overcontact binaries should merge and form a fast rotating star, but it has been suggested that $q_{\rm critical}$ can continue to fall up to 0.05 depending on the primary's mass and structure. Moreover, the obtained fill-out factors (50%–70%) indicate that mass loss is considerable and hydrodynamical simulations advocate that mass loss from L_2 is mandatory for a successful merging process. Comprehensively, the results indicate that ASAS J083241+2332.4 is at a stage of merger. The pivotal role played by the subtle nature of the derived mass ratio in forming a rapidly rotating star has been discussed.

Key words: binaries: close – binaries: eclipsing – binaries: general – stars: individual (ASAS J083241+2332.4)

Supporting material: data behind figure

1. INTRODUCTION

Overcontact binary systems form a very unique class of eclipsing binaries with very low angular momentum and are vaguely understood in terms of the nature of its progenitor and subsequent evolution. Their period varies from 1 to 0.19 days, surpassing the cut-off period limit (Nefs et al. 2012; Drake et al. 2014). These systems consist mainly of main-sequence stars of spectral type A–K, but recent surveys show that overcontact binary systems also host M spectral type stars (Nefs et al. 2012; Drake et al. 2014). Both the components in these systems are surrounded by a common convective envelope occupying a region from the inner to outer Lagrangian points often known as Roche lobes and hence have almost similar surface temperatures (Mochnacki 1981). It is observed that the secondary is at an advanced evolutionary stage owing to its oversized nature in comparison to its ZAMS radius (Stepien 2006). The study of overcontact binary systems is crucial in understanding many astrophysical problems, such as the process of merging and the related driving mechanism (e.g., Tylenda et al. 2011), the underlying dynamo cycle, the mass transfer phenomenon, and the presence of a third body (Eggleton & Kisseleva-Eggleton 2006), possibly explaining the low angular momentum in these systems. Broadly, overcontact binary systems fall into three categories: A-type, W-type (Binnendijk 1970), and H-type (Csizmadia & Klagyivik 2004). Though these subtypes have observational differences in terms of period and mass ratio, the true understanding of their evolutionary status is still unclear (Hilditch 1989; Gazeas & Niarchos 2006).

So far, only a few tens of overcontact binaries having low mass ratios (<0.25) and high fill-out factors ($f \gtrsim 50\%$) have been identified. Such a configuration is considered to be necessary for mergers and they are probable progenitors of FK Com-type and blue stragglers (Qian et al. 2006; e.g., see Kandulapati et al. 2015 for a list of such contact binary sources). It is very likely that a short period system with a low mass ratio is a prerequisite to form a single fast rotating star after merging. However, there are a few systems that have extremely low mass ratios: V53 ($q = 0.060$, a member of cluster M4, Kaluzny et al. 2013), SX Crv ($q \sim 0.066$, Rucinski et al. 2001 and $q \sim 0.072$, Zola et al. 2004), V857 Her ($q = 0.065$, Qian et al. 2005), AW UMa ($q = 0.080$, Pribulla et al. 1999), and V870 Ara ($q = 0.082$, Szalai et al. 2007). These systems challenge existing theoretical models, which predict that an overcontact binary system would merge around $q \sim 0.07$–0.09 (Rasio & Shapiro 1995; Li & Zhang 2006; Arbutina 2007, 2012). However, Jiang et al. (2010) argue that the minimum mass ratio can fall up to $q = 0.05$ and it depends on the primary's mass and structure. The discovery of such extreme mass ratio overcontact binaries is vital to resolve this ambiguity and refine the current theoretical models. The widely accepted mechanism for the process of merger is Darwin's instability model, wherein $J_{\rm rot} > 1/3\ J_{\rm orb}$ (where $J_{\rm rot}$ is the rotational angular momentum and $J_{\rm orb}$ is the orbital angular momentum; Hut 1980) triggers the binary to merge (Rasio & Shapiro 1995).

The Hα spectral line observed in overcontact binaries is an indicator of the presence of magnetic activity (Barden 1985; Kaszas et al. 1998; Kandulapati et al. 2015). The presence of stellar spots causes the filling of the Hα line, thus relatively decreasing its width. Based on a small sample of overcontact binaries, Kandulapati et al. (2015) found a correlation between the equivalent width (EW) of the Hα line and the orbital period

Table 1
Details of Variable (V1), Comparison, and Check Stars

Name	α_{J2000}, δ_{J2000}	V	J–H	V–K
ASAS J083241+2332.4 (variable V1)	$08^h\ 32^m\ 41\overset{s}{.}1$, $+23°\ 33'\ 12''$	12.60	0.27	1.42
Comparison star	$08^h\ 32^m\ 33\overset{s}{.}2$, $+23°\ 35'\ 20\overset{''}{.}1$	…	0.28	…
Check star	$08^h\ 32^m\ 31\overset{s}{.}7$, $+23°\ 35'\ 58\overset{''}{.}2$	…	0.36	…

of the system. In overcontact binaries, the presence of spots over the stellar surface causes an asymmetry in the light curve at phases 0.25 and 0.75, which is known as the O' Connell effect (O'Connell 1951; Milone 1969; Davidge & Milone 1984). Theoretical and observational studies show that magnetic activity is mostly associated with the primary component rather than the secondary due to deeper convective zones (Rucinski 1992, 1994; Kaszas et al. 1998; Vilhu & Maceroni 2007).

We performed R- and V-band photometry of a new overcontact binary system ASAS J083241+2332.4 (hereafter V1). The ASAS survey and Pepper et al. (2008) first reported the nature and variability of V1. However, fine features of the light curve could not be clearly observed due to large scatter. Since the system exhibits total eclipses, the photometric solution can reliably determine its mass ratio and inclination (Mochnacki & Doughty 1972; Terrell & Wilson 2005). Since the Hα line is an important diagnostic tool to understand the magnetic activity over the stellar surface, we have also studied the variation of this line along the orbital phase of the system.

2. OBSERVATIONS, DATA REDUCTION, AND ANALYSIS

R-band photometric observations were made using the 2 m telescope of the IUCAA-Girawali Observatory (IGO) from 2015 February 4–16 for five nights, and V-band observations were made during the night of 2015 February 16. The 2 K × 2 K, thinned, back-illuminated CCD, with a pixel size of 13.5 μm, a gain of 1.5e^-/ADU, and a read out noise of 4e^-, of the IUCAA Faint Object Spectrograph and Camera was used for imaging. This gives a plate scale of 0.3 arcsec pixel^{-1} and an image of size 10′ × 10′. Images were obtained with an integration time of 20–30 s in Bessell's R and V band. In order to perform differential photometry, we chose comparison and check stars that are close to the variable and lie in the same frame. Table 1 provides the position, color indices, and other parameters for all three stars. Differential magnitude light curves of variable versus comparison star and comparison versus check star are shown in Figure 1 (for 2015 February 8). The magnitude difference between the comparison and check star is found to be constant with an uncertainty of 0.008. The complete normalized light curve is shown in Figure 4 and corresponding data is available online.

Spectroscopic observations were performed on 2015 January 29 and 30, with the Himalaya Faint Object Spectrograph Camera mounted on the 2 m Himalaya Chandra Telescope (HCT), of the Indian Astronomical Observatory. It is equipped with a 2K × 4K CCD and a central region of 2K × 2K along with a plate scale of 0.″296/pixel that yields a 10′ × 10′ field of view. Data were obtained using a combination of a slit (width 1.″92 × 11′) and Grism 7, spanning a wavelength range of 3500 Å–7500 Å. This gives a dispersion of 1.5 Å/pixel and a resolution of ∼11 Å. An exposure time of 30–40 minutes was given for both the variable V1 and the spectrophotometric standard (BD+08 2015). The *FeAr* arc lamp was used for wavelength calibration. The IRAF[3] package and different sub-packages were used for reducing the data to obtain magnitudes and spectra. Spectra were normalized thereafter for further studies.

2.1. Period Analysis and Determination of Ephemeris

The *Period04* package (Lenz & Breger 2005) was employed to redetermine the period of the variable and the times of minima were obtained by the Kwee & van Woerdens method (Kwee & van Woerden 1956). The ephemeris for the variable based on our and Pepper's epoch (Pepper et al. 2008) are $\mathrm{Min}_I = 2457062.2450(22) + 0\overset{d}{.}311329(8)\mathrm{E}$ and $\mathrm{Min}_I = 2453415.8500(43) + 0\overset{d}{.}311321(3)\mathrm{E}$ respectively.

A similar period was also obtained from the ASAS data. Since most of the contact binaries show secular period variations, we used the times of minima from our R-band observations, ASAS data, and Pepper's data (Pepper et al. 2008; listed in column 1 of Table 2). The corresponding $(O-C)_1$ values obtained using our epoch for the variable are shown in column 3 of Table 2. The $(O-C)_1$ variation shows an upward trend of a quadratic nature, which is represented by a thick line (Figure 2(a), top panel). The residuals clearly suggest that there is an inherent systematic variation in the $(O-C)_1$ diagram and hence a quadratic function along with a sin term (A× sin ($\omega \times E + \omega_o$) was used to fit the overall $(O-C)_1$ variation (represented by a dashed line). We used the nonlinear squares method with an option robust=on to obtain the best fit, which uses the bi-square weights method along with Levenberg–Marquardt algorithm in the curve fitting toolbox package of MATLAB. The best-fit equations obtained using the times of minima derived from our and Pepper's epoch are as follows:

$$\begin{aligned}(O-C)_1 = {} & 0.01077(\pm 0.00096) + 5.311(\pm 0.259) \\ & \times 10^{-6} \times E + 3.772(\pm 0.175) \times 10^{-10} \\ & \times E^2 + 0.00281(\pm 0.0001) \times \sin(0\overset{\circ}{.}03718 \\ & \times (\pm 0\overset{\circ}{.}00068) \times E + 126\overset{\circ}{.}725(\pm 16\overset{\circ}{.}900))\end{aligned} \quad (1)$$

$$\begin{aligned}(O-C)_1 = {} & 0.0003121(\pm 0.000078) - 3.528(\pm 0.018) \\ & \times 10^{-6} \times E + 3.776(\pm 0.172) \\ & \times 10^{-10} \times E^2 + 0.002702(\pm 0.0003) \\ & \times \sin(0\overset{\circ}{.}0367(\pm 0\overset{\circ}{.}0017) \times E \\ & + 54\overset{\circ}{.}288(\pm 6\overset{\circ}{.}302)).\end{aligned} \quad (2)$$

The fit clearly shows that a long-term secular period increase at the rate of $dP/dt = 0.076 \pm 0.003$ s years^{-1} is superimposed by a periodic variation with an amplitude of ∼0.0028 days and a period of ∼8.25 years (Figure 2(a), top panel). Thick lines and dotted lines are the quadratic and the quadratic + sine terms respectively. Figure 2(a) (middle panel, $(O-C)_2$ diagram) gives the observed variation after subtraction of the quadratic variation and is fitted with a sine term (represented by a dashed line). Final residuals (Figure 2(a) bottom panel) do not indicate any systematic variation. A similar procedure was followed on

[3] IRAF is distributed by the National Optical Astronomy Observatory, which is operated by the Association of Universities for Research in Astronomy (AURA) under cooperative agreement with the National Science Foundation.

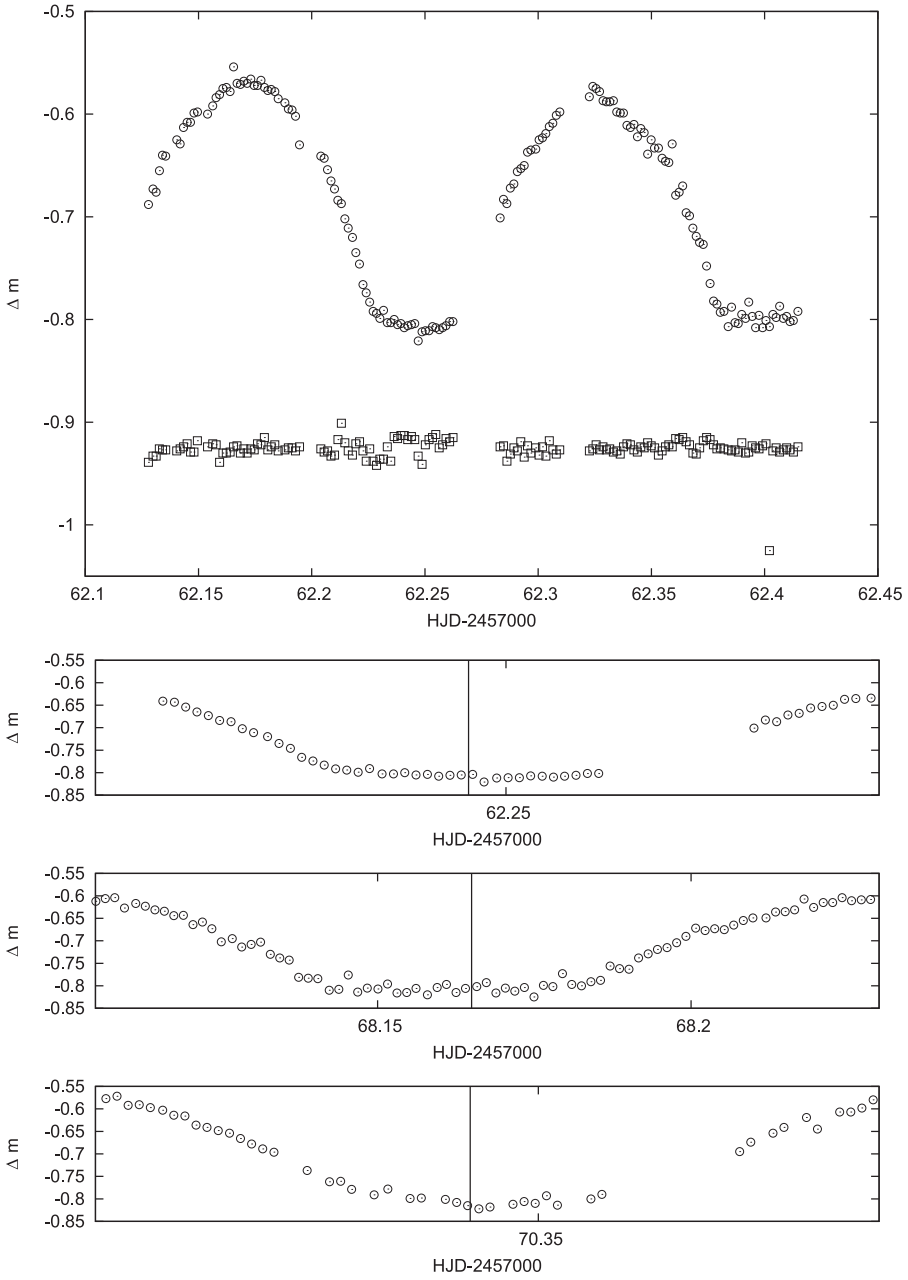

Figure 1. Top panel: magnitude difference of the variable—comparison (circles) and check—comparison (squares) observed on 2015 February 08 for R band. Bottom panels: samples of individual eclipse light curves. Vertical lines represent times of minima.

the O–C values obtained using Pepper's ephemeris and are shown in Figure 2(b).

Assuming that the periodic variation is caused by the presence of a third body, a similar approach is taken to constrain its orbital elements (middle panel in Figures 2(a) and (b)). The third body displaces the epochs of minimum light in a sinusoidal form, with a period equal to the orbital period of the third body, causing the Light Time Effect (LITE; Woltjer 1922; Irwin 1959). The time of mid-eclipse can be computed using

$$\text{Min.}I = JD_o + P.\,E + Q.\,E^2 + \frac{a_{12}\sin i}{c} \times \left[\frac{1-e_3^2}{1+e_3\cos\nu}\sin(\nu+\omega_3) + e_3\sin(\omega_3)\right], \quad (3)$$

where e_3, ω_3, ν, $a_{12}\sin i$, and c are the eccentricity, longitude of the periastron, true anomaly of the binary orbit around the center of mass of the triple system, projected semimajor axis, and the speed of light, respectively.

We implemented a MATLAB program based on Irwin's method (Irwin 1959) developed by Zasche et al. (2009). This program uses the Simplex method in order to arrive at the best solution. Figure 3 shows the LITE fit and the corresponding residuals. The orbital period thus derived is 8.95 ± 0.95 years, which is in good agreement with the one obtained from Equation (1). An eccentricity of $e = 0.47 \pm 0.10$ was also obtained. Other basic parameters like $a_{12}\sin i$, $f(M_3)$ and the mass of the third body for various inclinations are similar to those obtained from our ephemeris (see Table 3).

Table 2
Observed Times of Minima for Variable V1 from ASAS Database (1), Pepper's Data (2), and Our Observations (3)

HJD 2400000+	Error	Epoch	$(O-C)_1$	$(O-C)_2$	References	HJD	Error	Epoch	$(O-C)_1$	$(O-C)_2$	References
2622.91990	0.00850	−14259.5	0.00948	−0.00231	1	3474.68800	0.00081	−11523.5	−0.00464	−0.00431	2
2640.97650	0.00800	−14201.5	0.00929	−0.00220	1	3730.60070	0.00830	−10701.5	−0.00020	0.00262	1
2665.72650	0.00760	−14122	0.00904	−0.00207	1	3762.82240	0.00730	−10598	−0.00052	0.00261	1
2678.02380	0.00810	−14082.5	0.00904	−0.00186	1	3765.62430	0.00780	−10589	−0.00054	0.00263	1
2717.87280	0.00900	−13954.5	0.00858	−0.00158	1	3780.72340	0.00830	−10540.5	−0.00064	0.00266	1
2965.06190	0.00750	−13160.5	0.00650	0.00023	1	3789.59600	0.00880	−10512	−0.00078	0.00253	1
2966.30720	0.00820	−13156.5	0.00650	0.00025	1	3793.02060	0.00770	−10501	−0.00074	0.00266	1
2975.95810	0.00800	−13125.5	0.00636	0.00029	1	3795.35550	0.00740	−10493.5	−0.00077	0.00258	1
2998.52890	0.00750	−13053	0.00618	0.00042	1	4125.97860	0.00750	−9431.5	−0.00366	0.00203	1
3044.44880	0.00810	−12905.5	0.00580	0.00068	1	4128.46920	0.00890	−9423.5	−0.00365	0.00205	1
3053.63270	0.00860	−12876	0.00565	0.00061	1	4174.54470	0.00850	−9275.5	−0.00409	0.00191	1
3060.48180	0.00880	−12854	0.00562	0.00071	1	4466.56400	0.00780	−8337.5	−0.00662	0.00066	1
3069.19880	0.00850	−12826	0.00555	0.00083	1	4478.23850	0.00880	−8300	−0.00676	0.00050	1
3099.08500	0.00810	−12730	0.00466	0.00035	1	4491.93660	0.00890	−8256	−0.00692	0.00044	1
3109.51490	0.00880	−12696.5	0.00520	0.00099	1	4508.28100	0.00880	−8203.5	−0.00702	0.00039	1
3124.45830	0.00750	−12648.5	0.00506	0.00110	1	4512.32820	0.00810	−8190.5	−0.00703	0.00040	1
3331.17560	0.00840	−11984.5	0.00328	0.00195	1	4519.48860	0.00730	−8167.5	−0.00708	0.00032	1
3338.80300	0.00750	−11960	0.00325	0.00194	1	4523.38010	0.00880	−8155	−0.00713	0.00033	1
3340.98220	0.00880	−11953	0.00318	0.00196	1	4529.45080	0.00720	−8135.5	−0.00725	0.00025	1
3347.67560	0.00780	−11931.5	0.00311	0.00194	1	4539.72440	0.00770	−8102.5	−0.00734	0.00017	1
3348.60960	0.00870	−11928.5	0.00314	0.00195	1	4556.22450	0.00820	−8049.5	−0.00740	0.00011	1
3363.55300	0.00890	−11880.5	0.00299	0.00203	1	4561.67260	0.00830	−8032	−0.00747	0.00003	1
3404.49170	0.00770	−11749	0.00260	0.00211	1	4795.00780	0.00790	−7282.5	−0.00954	−0.00162	1
3407.76060	0.00700	−11738.5	0.00260	0.00214	1	4813.99840	0.00800	−7221.5	−0.00970	−0.00181	1
3410.87380	0.00850	−11728.5	0.00256	0.00218	1	4822.09280	0.00770	−7195.5	−0.00972	−0.00181	1
3415.85000	0.00072	−11712.5	−0.00242	−0.00276	2	4836.88050	0.00820	−7148	−0.00991	−0.00200	1
3432.81800	0.00071	−11658	−0.00158	-0.00177	2	4851.51270	0.00790	−7101	−0.00993	−0.00200	1
3436.55780	0.00081	−11646	0.00234	0.00217	2	4853.69190	0.00760	−7094	−0.01000	−0.00210	1
3438.73700	0.00076	−11639	0.00227	0.00219	2	4865.36640	0.00750	−7056.5	−0.01015	−0.00220	1
3440.75700	0.00085	−11632.5	−0.00134	−0.00138	2	4895.40890	0.00790	−6960	−0.01040	−0.00250	1
3442.78500	0.00078	−11626	0.00306	0.00304	2	4921.09290	0.00880	−6877.5	−0.01063	−0.00270	1
3445.73700	0.00087	−11616.5	−0.00252	−0.00253	2	7058.35000	0.00085	−12.5	0.00783	−0.00290	3
3460.67800	0.00089	−11568.5	−0.00507	−0.00496	2	7062.24500	0.00080	0	0.01128	0.00053	3
3464.72000	0.00082	−11555.5	−0.01028	−0.01012	2	7062.39500	0.00090	0.5	0.00562	−0.00517	3
3466.74800	0.00093	−11549	−0.00588	−0.00570	2	7065.36000	0.00081	10	0.01304	0.00218	3
3467.69000	0.00084	−11546	0.00215	0.00231	2	7068.16500	0.00088	19	0.01613	0.00523	3
3469.70800	0.00086	−11539.5	−0.00346	−0.00326	2	7070.18500	0.00086	25.5	0.01252	0.00159	3
3472.67100	0.00080	−11530	0.00196	0.00227	2	7070.34000	0.00080	26	0.01186	0.00099	3
3473.75400	0.00078	−11526.5	−0.00467	−0.00442	2						

2.2. Photometric Solution Using Wilson Devinney Method

The R- and V-band light curves of V1 show total eclipses along with a trace of the O'Connell effect at phase 0.25. Totality suggests that it is a low mass ratio system ($0.1 < q < 0.2$) (Terrell & Wilson 2005; Wilson 2006). Based on J–H and V–K color indices, the effective temperature of the primary component was fixed at 6300 K (Cox 2000). We obtained the photometric solution using the Wilson–Devinney (W–D) code (Wilson & Devinney 1971; Wilson 1979, 1990; Wilson & van Hamme 2003). The following methodology is adopted to obtain the best solution (e.g., Sriram et al. 2009; Kiron et al. 2011, 2012; Kandulapati et al. 2015). Similar temperatures of the primary and secondary component indicate the presence of a common convective envelope, hence throughout the computations we fixed the gravity darkening co-efficients $g_1 = g_2 = 0.32$ (Lucy 1967) and bolometric albedos $A_1 = A_2 = 0.5$ (Rucinski 1969). Limb darkening coefficients of the components x_1 and x_2 were fixed at 0.62 (Van Hamme 1993) for R band. A synchronous and circular orbit was assumed for the computation. In order to obtain the photometric solution, four parameters were adjusted in the code: temperature of the secondary component (T_2), orbital inclination (i), the dimensionless potentials of the primary and secondary components ($\Omega_1 = \Omega_2$), and the bandpass luminosity of the primary star (L_1).

Previously, this variable was not spectroscopically studied, but the observed light curve shows total eclipses and hence the photometrically determined values of inclination and mass ratio can be considered reliable (Mochnacki & Doughty 1972; Terrell & Wilson 2005). The grid search method was adopted to constrain the mass ratio (q) and the best solutions were obtained for q ranging from $0.04 < q < 10.0$, by allowing the adjustable parameters to vary. The computations favored mode 3 (overcontact) over mode 2 (detached). Finally, the mass ratio parameter was also freed along with other adjustable parameters in the differential correction (DC) program. High residuals at phase 0.25 of the variable V1 indicated the presence of a cool or hot spot and hence a solution with a cool and hot spot over the surface of the primary was incorporated to obtain the final parameters, which resulted in the lowering of the residuals $(\sum (\omega(o - c))^2$, was found to be 0.0068 for the

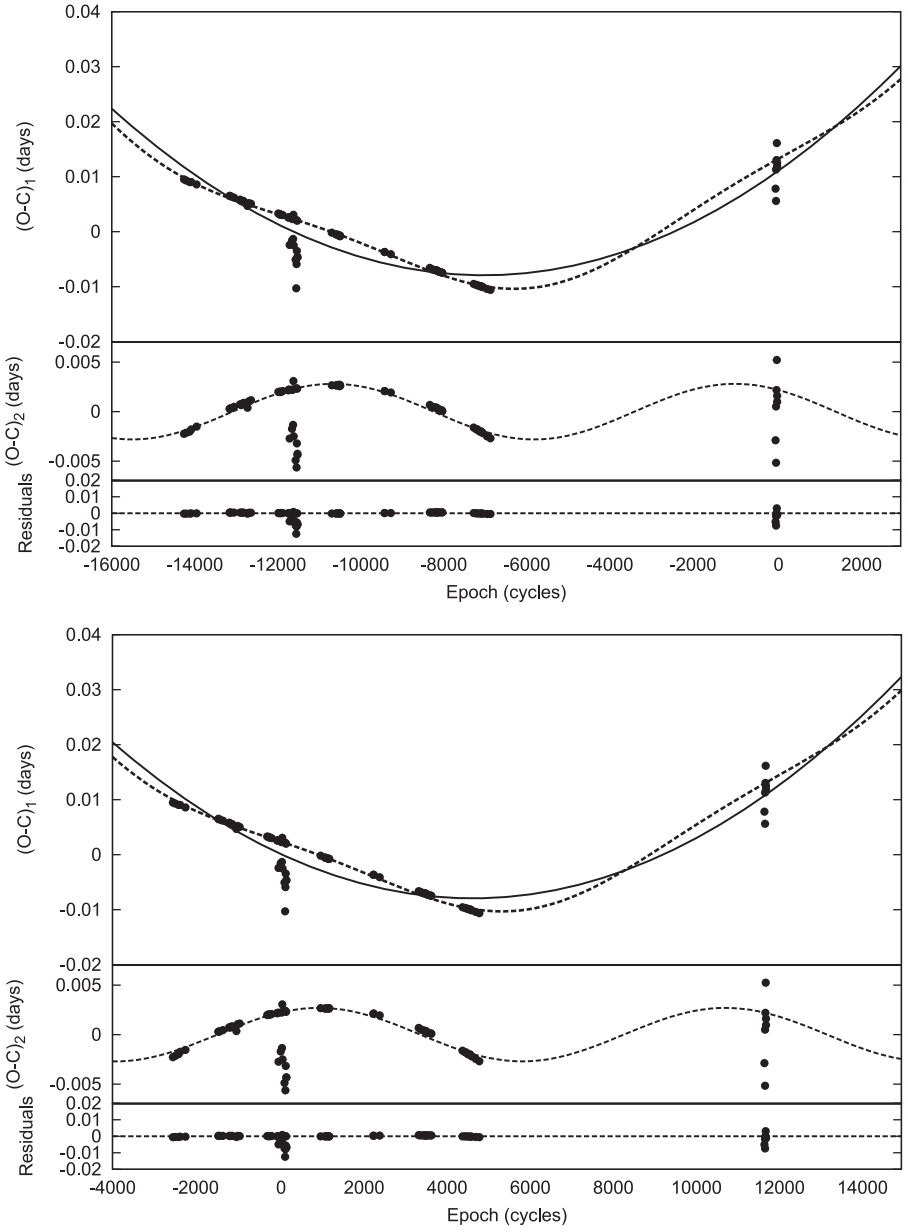

Figure 2. Top (a): the O–C diagram along with the quadratic fit (thick line) and quadratic + sin term (dashed line) using Equation (1) (see the text). The second panel is the residual after removing the quadratic term, which is then fitted with the function $A^*\sin(\omega^* E + \omega_o)$ (dashed line). The last panel is the final residual showing no significant variation. Bottom (b): similar figure with O–C diagram obtained with Pepper's ephemeris using Equation (2) (see the text).

cool spot solution and 0.0062 for the hot spot solution (see Table 4)). The hot spot solution was anticipated based on the O–C diagram, which showed an increase in the orbital period of the binary indicating that mass transfer is from the secondary to the primary component. Best fit solutions resulted in a mass ratio of $q = 0.0652 \pm 0.0013$, inclination $i = 82\overset{\circ}{.}74 \pm 1.14$ (cool spot) and $q = 0.0677 \pm 0.0014$, inclination $i = 82\overset{\circ}{.}67 \pm 1.09$ (hot spot). In order to check the consistency of the solution, temperature and inclination were varied by 5%–10% and no significant differences were observed in the final solution. In the W–D code, a spot is characterized by four parameters, i.e., the latitude of a star spot center (measured from 0 radians at the north pole to π radians at the south pole), the longitude of a spot center (measured counter-clockwise from the line of the star center from 0° to 360°), the angular radius of a star spot in degrees and $T_{\rm spot}/T_*$ (ratio of the spot temperature to the ambient stellar surface temperature). Obtained spot parameters for a cool spot solution are, colatitude $= 59\overset{\circ}{.}58 \pm 1\overset{\circ}{.}73$, longitude $= 293\overset{\circ}{.}41 \pm 2\overset{\circ}{.}19$, radius $= 8\overset{\circ}{.}59 \pm 0\overset{\circ}{.}57$, and $T_{\rm spot}/T_* = 0.80 \pm 0.03$ and those for a hot spot solution are colatitude $= 59\overset{\circ}{.}58 \pm 3\overset{\circ}{.}27$, longitude $= 87\overset{\circ}{.}02 \pm 1\overset{\circ}{.}15$, radius $= 10\overset{\circ}{.}31 \pm 0\overset{\circ}{.}42$, and $T_{\rm spot}/T_* = 1.100 \pm 0.008$. Based on the solutions, the observed O'Connell effect can fairly equivalently be modeled by a cool or hot spot and each solution relies on a different physical effect for explanation. It is very likely that in reality, the observed O'Connell effect is actually a more complicated combination of cool and hot spots, as well as other physical variations.

To verify the uniqueness of the final solutions, we employed PHOEBE's scripter capabilities (Prsa & Zwitter 2005) and performed a Monte-Carlo parameter scan (heuristic scanning

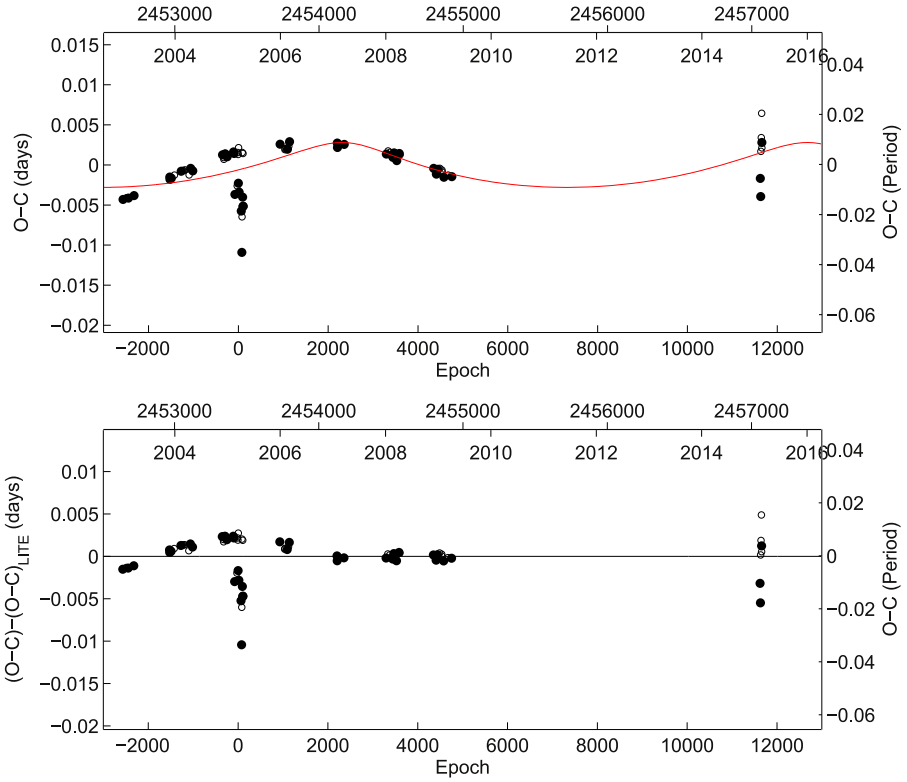

Figure 3. Top: circles represent the O–C residual obtained from the quadratic term in Equation (3) and the thick line shows the possible modulation due to the light time effect (LITE) due to a third body. The bottom panel is the residual after considering LITE.

method) using DC minimization. DC minimization was performed for 1000 iterations, each time updating all of the adjustable parameters (T_2, i, q, and Ω) based on the previous iteration (Bonanos 2009; Maceroni et al. 2009). For each of the adjustable parameters, histograms were obtained for which the mean and standard deviations are reported (Table 4). Figure 5 shows the Gaussian fitted histograms for secondary component temperature (T_2 K) and mass ratio q for the cool spot solution.

2.3. Study of the Hα 6563 Å Line

Observations of the Hα line at various phases of the variable were studied in order to detect any fill-in effect. Figure 6 (top panel) gives the Hα line of the variable and the standard star at phases ∼0.25 and ∼0.75. No significant fill-in effect is observed for the variable, indicating that there is no substantial magnetic activity presently associated with the variable. Although the system shows a trace of the O' Connell effect, it is probably not enough to reflect in the Hα line profile. The mean EW was found to be 2.51 ± 0.20 Å. In the case of a contact binary system, the observed EW is affected by the temperature of the components and the mass ratio of the system (Webbink 2003). Intrinsic EWs corresponding to the primary and secondary are $EW_p^i = a \times EW_p$ and $EW_s^i = a \times EW_s$, where $a = 1 + q^{0.92}\ (T_s/T_p)^4$ (Webbink 2003), EW_p and EW_s are measured equivalent widths and EW_p^i and EW_p^i are intrinsic EWs. Kandulapati et al. (2015) found that there exists a correlation between the orbital period of the system and the EW of the Hα line and hence the EW at ∼0.5 phase of V1 is plotted in a period-EW plane (Figure 6, bottom panel). It is clear from the figure that there is a direct correlation between the orbital period and EW. It is also noticed that the EW for V1 is relatively higher compared to those of other systems. We argue that it could possibly be due to the low magnetic activity of V1, which is causing the EW of the line to be broadened. As the activity increases, the EW of the Hα line narrows and gradually fills in. Further observations of the variable can help in understanding this phenomenon because contact binaries often show variable O'Connell effects.

3. DISCUSSION AND CONCLUSION

We performed R- and V-band photometry and Hα line analysis of a new contact binary ASAS J083241+2332.4. The variable exhibits totality in its light curve and a trace of the O'Connell effect is also found to be associated with it. The photometric solution suggests that V1 is an extremely low mass ratio system with $q \sim 0.06$ and an orbital inclination $i \sim 82°$. The fill-out factors were derived to be ∼51% and ∼69%, respectively, for cool spot and hot spot solutions, and the secondary component is found to be slightly hotter by $\Delta T \sim$ 300 K, which is characteristic of a W-type W UMa overcontact binary system. Such extremely low mass ratio binary systems are rare and only three such systems have been reported so far: V53 ($q = 0.060$; Kaluzny et al. 2013), V857 Her ($q = 0.065$; Qian et al. 2005), and SX Crv ($q = 0.072$; Zola et al. 2004). It should be noted that the mass ratio reported for SX Crv is spectroscopically determined (Zola et al. 2004) and those for other variables mentioned are based on photometry. Another striking aspect is that V1 closely resembles SX Crv in terms of its period, temperature of components, temperature difference, mass ratio, and fill-out factor despite the difference in the shape of the observed light curve, i.e., V1 shows total eclipses and a trace of the O'Connell effect, whereas SX Crv does not show totality and has a relatively strong O'Connell effect (Zola et al. 2004). Moreover, the period of SX Crv shows a secular

Table 3
Third Body Solution Obtained from Equations (1)–(3)

Parameters	Our Ephemeris	Pepper's Ephemeris
Solution Using Equations (1) and (2) (See Text)		
A, semi. amplitude (days)	0.00281 ± 0.0001	0.002702 ± 0.000601
ω (degrees)	0.0371 ± 0.0007	0.0367 ± 0.0034
ω_o (degrees)	126.725 ± 16.901	54.28 ± 12.97
P_3, period (years)	8.25 ± 0.148	8.34 ± 0.89
a_{12}sin i, (AU)	0.488 ± 0.018	0.470 ± 0.104
$f(M_3)$, $(M_\odot)$	0.00172 ± 0.00033	0.00153 ± 0.00038
M_3 $(M_\odot)_{i=90^\circ}$	0.16 ± 0.01	0.153 ± 0.012
M_3 $(M_\odot)_{i=60^\circ}$	0.19 ± 0.01	0.174 ± 0.018
M_3 $(M_\odot)_{i=30^\circ}$	0.35 ± 0.02	0.329 ± 0.026
Light Time Effect Solution Using Pepper's Ephemeris and Zasche's Code		
A, semi. amplitude (days)	0.0028 ± 0.0006	⋯
P_3, period (years)	8.95 ± 0.59	⋯
e_3, eccentricity	0.47 ± 0.09	⋯
ω_3, longitude of periastron passage	107.01 ± 22	⋯
T_o, time of periastron passage	2454258.882 ± 359.94	⋯
a_{12}sin i, (AU)	0.489 ± 0.09	⋯
$f(M_3)$, $(M_\odot)$	0.00146 ± 0.00098	⋯
M_3 $(M_\odot)_{i=90^\circ}$	0.153 ± 0.03	⋯
M_3 $(M_\odot)_{i=60^\circ}$	0.178 ± 0.04	⋯
M_3 $(M_\odot)_{i=30^\circ}$	0.33 ± 0.07	⋯

decrease (Zola et al. 2004). V857 Her, having a period of 0.3822 days, has a relatively early spectral type A7 (Pribulla & Rucinski 2008). The light curve of V857 Her observed on 2002 April 22, and 2002 May 6 and 7, (http://www.astro.sk/~pribulla/roztoky.html) and that observed by Qian et al. (2005) from 2005 February 7–9, clearly show a variable O'Connell effect, which suggests that there exists a faster dynamo cycle in V857 Her. The O–C study for V857 Her indicates that its period is increasing (Qian et al. 2005).

The theoretical critical mass ratio for a contact binary system to merge is predicted to be about $q_{\rm critical} \sim 0.07$–$0.09$ (Rasio & Shapiro 1995; Li & Zhang 2006; Arbutina 2007, 2012) and systems discussed above challenge the existing theoretical models. If the secondary star's rotation is neglected, then the critical mass ratio is found to be about $q_{\rm critical} = 0.09$ (Rasio 1995) and this value decreases to $q_{\rm critical} = 0.076$ otherwise (Li & Zhang 2006). Assuming a radiative main-sequence nature for the primary star and a convective nature for the secondary star, we can arrive at a critical mass ratio range of about $q_{\rm critical} = 0.094$–0.109 (Arbutina 2007, 2012). Considering the differential rotation of the primary star, which enhances the central concentration results in $q_{\rm critical} = 0.076$ (Arbutina 2009), Jiang et al. (2010) demonstrated that the dimensionless radius of gyration k^2 $(=\frac{I}{MR^2})$ of a system decreases with an increase in its age and mass (if $\leqslant 1.3\ M_\odot$), leading to a critical mass ratio in the range of $0.05 < q_{\rm critical} < 0.105$. Comprehensively, it was suggested that the low value of $q_{\rm critical}$ ultimately depends on the structure of the primary star and the degree of contact of the overcontact binary system (Rasio & Shapiro 1995; Li & Zhang 2006; Jiang et al. 2010).

Theoretical studies indicate that overcontact binary systems would eventually coalesce and form a single fast rotating star (Webbink 1976; Mateo et al. 1990; Stepien 2012) and dynamical instability would be triggered if the fill-out factor (f) exceeds 70% or 86% (Rasio & Shapiro 1995; Li & Zhang 2006). The above ambiguity in f value is due to the consideration of loss of angular momentum because of gravitational wave radiation or magnetic stellar winds (Li & Zhang 2006). However, there exists only one observation that supports this scenario, i.e., V1309 Sco (Tylenda et al. 2011) and calculations suggest that a low mass ratio ($q = 0.10$) contact binary configuration was achieved by this system just before the merger (Stepien 2011). Nandez et al. (2014) performed a hydrodynamical simulation of this system and concluded that the Darwin instability played a vital role in the process of merger along with the loss of mass from L_2 (second Lagrangian point) just a few days before the merger. In our previous study, based on a sample of systems having a low mass ratio ($q < 0.25$) and a high fill out factor ($f > 50\%$), we reported possible observational evidence of a critical mass ratio of about $q_{\rm critical} = 0.085$ (Kandulapati et al. 2015), which is in close agreement with the theoretically predicted critical mass ratio range, $q = 0.07$–0.09 (Rasio & Shapiro 1995; Li & Zhang 2006; Arbutina 2007). Figure 7 shows the location of V1 on the log period–log mass ratio plane (triangle symbol). Two other low mass ratio systems have also been shown in the figure (inverted triangles): E48 ($p = 0.2829$ days, $q = 0.148$) and E53 ($p = 0.3084$ days, $q = 0.060$) (Kaluzny et al. 2013). Here, SX Crv (Zola et al. 2004) is represented by a diamond symbol. In this figure, V1 lies with a few other extreme low mass ratio systems and is found to be slightly away from the other systems.

The emission of the Hα 6563 Å line in overcontact binaries indicates the presence of magnetic activity in the chromosphere (Barden 1985) and, in general, that a Balmer series of hydrogen is the primary signature of radiation arising from the chromosphere of Sun-like stars (Linsky et al. 1982; Foukal 1990; Reid & Hawley 2005). In the case of V1, a trace of the O'Connell effect is observed, but a fill-in effect is not seen and the average EW is found to be 2.52 ± 0.22 Å. We argue that a threshold magnetic activity is required to cause the fill-in effect. In the case of ASAS J082243+1927.0, where the O'Connell effect

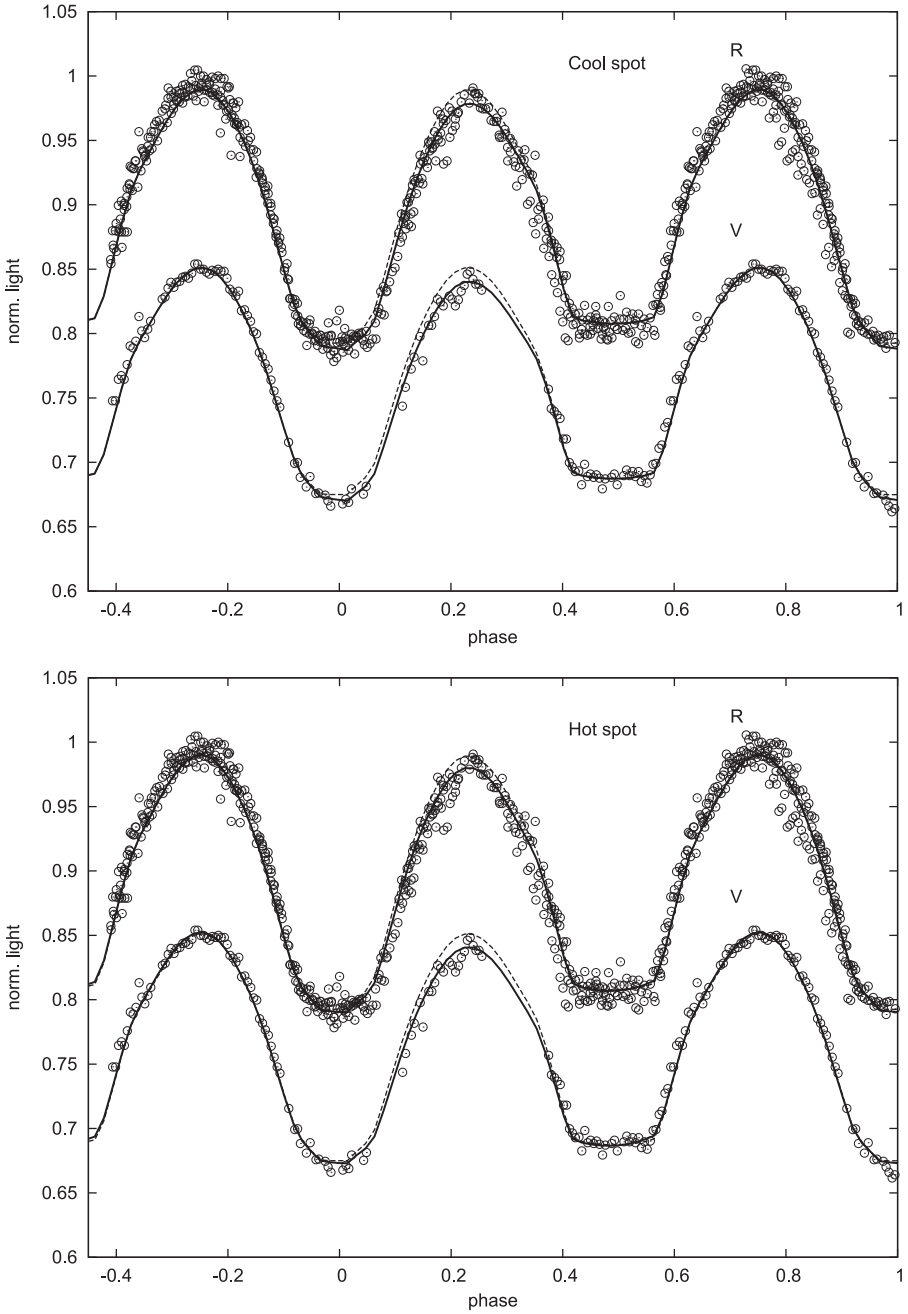

Figure 4. Top: R- and V-band light curves fitted using unspotted (dashed line) and cool spot (solid line) solutions (see the text). Bottom: similar figure with hot spot (solid line) solution.

(The data used to create this figure are available.)

was found to be prominent, visual inspection of the Hα line clearly revealed a fill-in effect (Kandulapati et al. 2015). The fill-in effect is observed in a few other overcontact binary systems, i.e., V566 Oph, AH Vir, W UMa (Barden 1985), and VW Cep (Frasca et al. 1996; Kaszas et al. 1998). This effect is associated with the primary component rather than the secondary, though the effective temperatures of both are similar. This is probably due to the underlying weak dynamo action resulting from a shallower convective zone in the secondary component (Vilhu & Rusinski 1983; Vilhu & Walter 1987; Webbink 2003). In our previous work, we found a correlation between period and intrinsic EW of the Hα 6563 Å line for a few contact binaries (Kandulapati et al. 2015). In the case of V1, we found that the correlation holds well but is less tight. The strong Hα absorption line is a signature of the zero point for chromospheric activity (Young et al. 1984). Stauffer & Hartmann (1986) argued that even a weak chromosphere can give rise to a weak Hα line. As the magnetic heating in the atmosphere increases, the absorption EW initially increases and later decreases, which causes the line to fill in, ultimately resulting in a pure emission line. Hence the observed higher EW for V1 is associated with a low magnetic activity and as the activity increases, the EW decreases, which leads to the fill-in effect. This would strengthen the observed correlation between the period and intrinsic EW of Hα line. Since a variable O'Connell effect was observed over a span of three years for a

Table 4
Photometric Solutions Obtained for Variable V1

Parameters		KP301148 (V1) Unspotted	Cool Spot	Hot Spot
$A_1 = A_2$		0.50	0.50	0.50
$g_1 = g_2$		0.32	0.32	0.32
T_1 (K)		6300	6300	6300
T_2 (K)		6602 ± 33	6667 ± 38	6672 ± 36
q		0.0671 ± 0.0016	0.0652 ± 0.0013	0.0677 ± 0.0014
i^o		81.95 ± 1.11	82.74 ± 1.14	82.67 ± 1.09
$\Omega_{1,2}$		1.8306 ± 0.0076	1.8229 ± 0.0079	1.8227 ± 0.0010
Fill-out factor (f %)		46.70 ± 2.12	50.65 ± 2.23	69.2 ± 2.54
r_1	pole	0.5642 ± 0.0024	0.5661 ± 0.0025	0.5669 ± 0.0003
	side	0.6439 ± 0.0044	0.6471 ± 0.0047	0.6488 ± 0.0006
	back	0.6610 ± 0.0052	0.6642 ± 0.0054	0.6668 ± 0.0008
r_2	pole	0.1768 ± 0.0110	0.1758 ± 0.0113	0.1816 ± 0.0027
	side	0.1850 ± 0.0134	0.1841 ± 0.0137	0.1907 ± 0.0033
	back	0.2286 ± 0.0390	0.2419 ± 0.0417	0.2450 ± 0.0130
$(L_1/L_1 + L_2)_V$		0.9260 ± 0.0038	0.9277 ± 0.0028	0.9082 ± 0.0034
$(L_1/L_1 + L_2)_R$		0.9125 ± 0.0032	0.9151 ± 0.0022	0.8999 ± 0.0033
Spot Colatitude (°)		...	59.58 ± 1.73	59.58 ± 3.27
Spot Longitude (°)		...	293.41 ± 2.19	87.02 ± 1.15
Spot Radius(°)		...	8.59 ± 0.57	10.31 ± 0.42
$T_{\rm Spot}/T_{\rm local}$		...	0.80 ± 0.03	1.100 ± 0.008
Σw(o–c)^2		0.007192	0.006807	0.006269

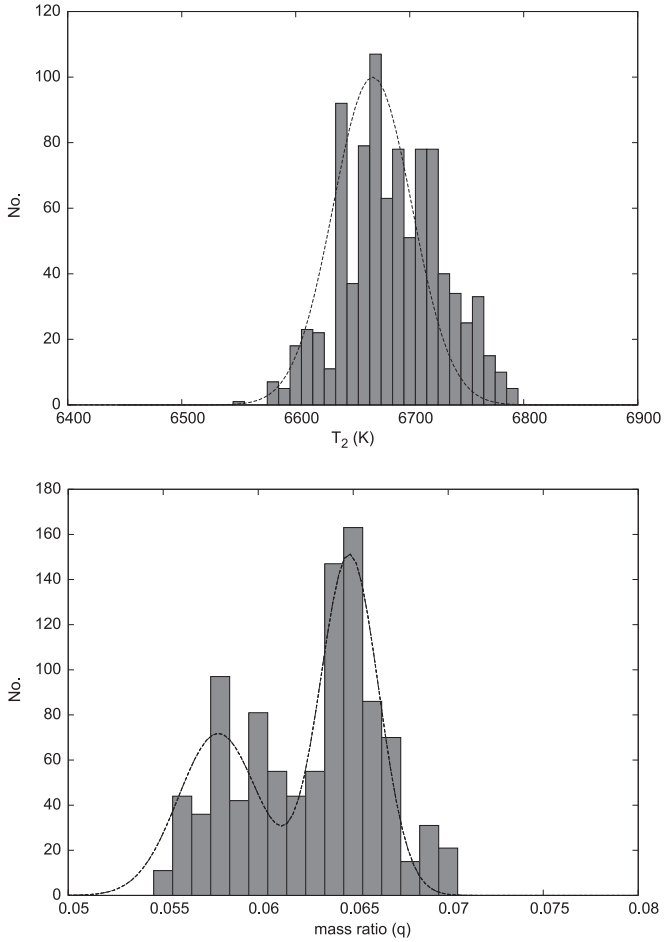

Figure 5. Gaussian fitted histograms of secondary temperature and mass ratio for the cool spot solution obtained using the Monte Carlo scan (see the text).

similar system, V857 Her (Qian et al. 2005), we speculate that the O' Connell effect would soon be stronger in V1.

The O–C residual diagram shows a systematic variation with a period of ∼8.25 years. Such a periodic modulation could be a result of the inherent magnetic activity of the system and can be explained using the Applegate mechanism (Applegate & Patterson 1987; Applegate 1992). The relative amplitude of period modulation of the cycle, $\Delta P/P = 2\ \pi$ (O–C)/$P_{\rm mod} = 1.605 \times 10^{-6}$ resulted in an orbital period variation of $\Delta P = 0.139$ s. The quadrupole moment (Lanza & Rodono 2002) is given by

$$\Delta Q = -\frac{\Delta P \times Ma^2}{9 \times P}, \quad (4)$$

where M is the mass of the active star and "a" is the semimajor axis of the orbit. By using the mass of the primary component, $M_1 = 1.33\ M_\odot$ (obtained from color indices), the quadrupole moment is found to be $\Delta Q_1 = 3.47 \times 10^{49}$ g cm^2 and for the secondary component mass $M_2 = 0.086\ M_\odot$, $\Delta Q_2 = 2.11 \times 10^{48}$ g cm^2. For the mass ratio derived from the hot spot solution, a similar value of $\Delta Q_2 = 2.20 \times 10^{48}$ g cm^2 was obtained. Owing to the remarkable resemblance of our variable to SX Crv, we have evaluated $\Delta Q_1 = 3.24 \times 10^{49}$ g cm^2 for $M_1 = 1.25\ M_\odot$ and $\Delta Q_2 = 2.55 \times 10^{48}$ g cm^2 for $M_2 = 0.098\ M_\odot$ (M_1 and M_2 being the masses of the primary and secondary components in SX Crv, Zola et al. 2004). ΔQ should be of the order of 10^{51-53} g cm^2 for the Applegate mechanism to play a role in the periodic modulation. Since ΔQ here is $\leqslant 10^{51-53}$ g cm^2, we conclude that the Applegate mechanism is not responsible for the observed periodic modulation. Moreover, Pribulla & Rucinski (2006) asserted that most of the overcontact binary systems host a third body.

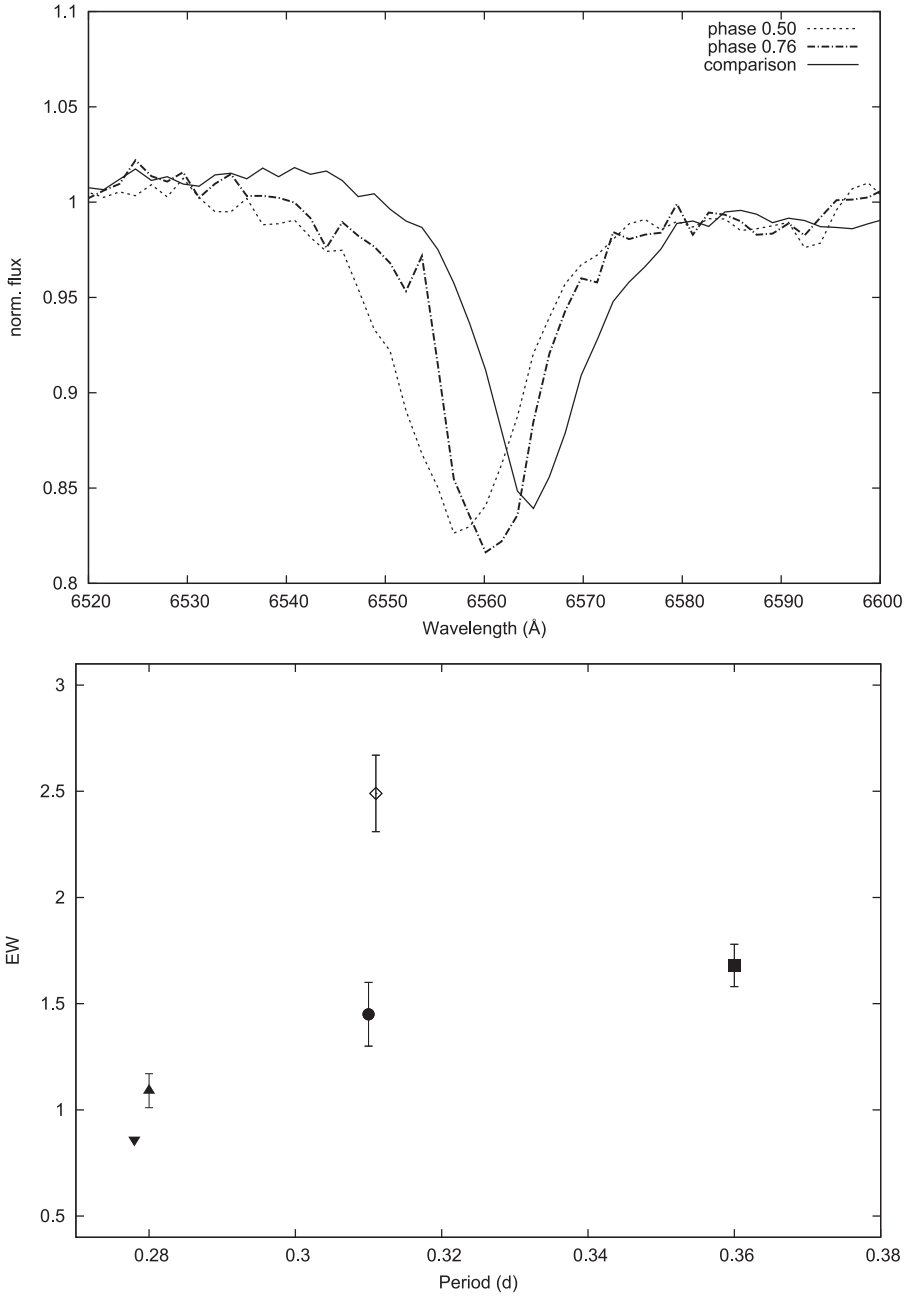

Figure 6. Top panel: comparison of the Hα line of the variable (at phases 0.50 and 0.76) and the standard star. Bottom panel: period vs. intrinsic equivalent width of the Hα line for overcontact binaries (see the text). Variable V1 is represented by the diamond symbol.

If the periodic variation is caused by the LITE due to the presence of a third body with $a_{12} \sin i \sim 0.49$ AU, then by using the following equation,

$$f(m) = \frac{(M_3 \sin i)^3}{(M_1 + M_2 + M_3)^2} = \frac{4\pi^2}{GP_3^2} \times (a_{12} \sin i)^3, \qquad (5)$$

a mass function of $f(m) = 0.0017\ M_\odot$ was obtained for the third body. For inclinations of $i = 90°$, 60°, and 30°, the mass of the third body is found to be $M_3 = 0.16\ M_\odot$, $M_3 = 0.19\ M_\odot$, and $M_3 = 0.35\ M_\odot$, respectively, for both cool and hot spot solutions. Similar values were obtained, using the $a_{12} \sin i$ derived from Pepper's ephemeris. A third light component was included in the solution, but it did not result in any significant variation in the parameters and was found to be zero (within the uncertainty limit). Assuming a mass range of 0.35–0.16 $M_\odot$, we have found that the third body is almost 50–500 times fainter (assuming a *M–L* relation for MS) than the close binary system. Hence it would be fainter by 6–9 mag compared to the close binary system. The secular period change observed in the O–C diagram suggests that the period is increasing at a rate of $dP/dt = 0.076\ \mathrm{s\ years}^{-1}$. Assuming a conservative mass transfer between the binary components, increase in the period suggests that mass is transferring from the secondary (less massive) component to the primary (more massive) component. From the following equation,

$$\frac{\dot{P}}{P} = -3\dot{M}_2 \left[\frac{1}{M_1} - \frac{1}{M_2}\right], \qquad (6)$$

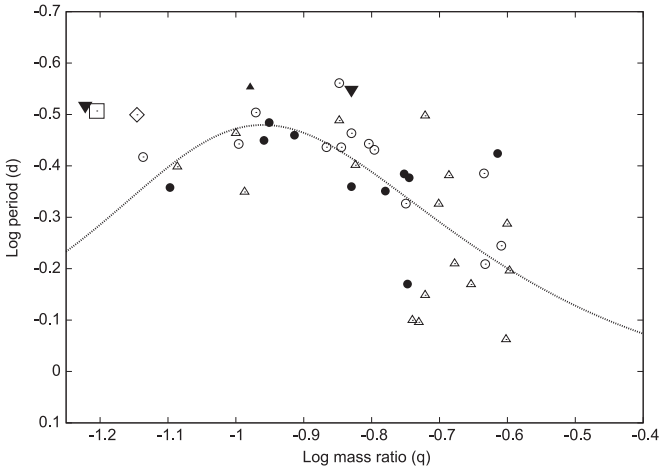

Figure 7. Mass ratio vs. period for low mass ratio overcontact binaries with high fill-out factors. Open and filled circles denote the secular period increase and decrease for the individual systems (see Table 3 and Figure 5 of Kandulapati et al. 2015). Box (Variable V1), diamond (SX Crv), and inverted triangles (E53 and E48 variables; see the text).

the mass transfer rate is determined to be $8.28 \times 10^{-8} M_{\odot}$ years^{-1}. A gradual increase in the orbital period causes a decrease in the magnitude of the mass ratio (q). Based on the conservative mass transfer phenomenon, further decrease in the mass ratio can cause the system to rapidly merge and form a fast rotating star.

Most of the theoretical models eventually predict a merger scenario for contact binary systems (Stepien 2012). For a system to merge, its orbital period must decrease and the associated responsible mechanisms are angular momentum loss (AML) due to stellar winds, mass loss from L_2, or gravitational wave radiation. The theoretical constraint on AML can be determined from the following equation (Bradstreet & Guinan 1994):

$$\frac{dP}{dt} \sim -1.1 \times 10^{-8} q^{-1}(1+q)^2 \times (M_1 + M_2)^{-5/3} k^2 (M_1 R_1^4 + M_2 R_2^4) P^{-7/3}. \quad (7)$$

Using $M_1 = 1.33\ M_{\odot}$, $M_2 = 0.086\ M_{\odot}$, $R_1 = 1.23\ R_{\odot}$, $R_2 = 0.110\ R_{\odot}$, $q = 0.065$, k^2 (gyration constant) $= 0.1$, and $P = 0.311321$ days (where M_1, M_2, R_1, and R_2 are obtained from color indices and the derived mass ratio), we obtained $dP/dt_{\rm theoretical} = -0.043$ s years^{-1} for cool spot solution (for the hot spot solution, a similar value of $dP/dt_{\rm theoretical} = -0.041$ s years^{-1} was obtained). Similarly, by using masses and radii of SX Crv, which seem to be applicable to this system, we obtained $dP/dt_{\rm theoretical} = 0.065$ s years^{-1} (Zola et al. 2004). It can be seen that the $|dP/dt_{\rm theoretical}|$ is found to be slightly lower, though not significantly, than the observed rate of change of period ($\sim$0.076 s years^{-1}). However, the obtained fill-out factors ($\sim$50%–70%) suggest that there is considerable mass loss from L_2 which is an important physical mechanism for AML/mass loss as well as for the merging process (Nandez et al. 2014).

Based on O–C diagrams in contact binaries, increase and decrease in period variations are often observed. Based on a study of 90 contact binaries, Rucinski et al. (2013) argued that these observed variations in contact binaries are not related to their evolutionary states. In contact binaries, there are two processes acting oppositely, expansion of the secondary component accompanied by mass transfer to the primary and AML (Gazeas & Stepien 2008). The former process tightens the orbit and the latter one widens it. This phenomena continues until the Hut's criteria is met and the system coalesces at the critical mass ratio (Rasio & Shapiro 1995; Li & Zhang 2006; Arbutina 2012; Jiang et al. 2010). In our case, the O–C diagram suggests that the orbital period is increasing and, as the system meets the Hut's criteria, it would eventually merge.

3.1. Distance and Absolute Parameters

Based on a sample of contact binaries, Gettel et al. (2006) derived an empirical relation to determine the distance to a system. Using the relation Log $D = 0.2\ V_{\rm max} - 0.18$ log $(P) - 1.60\ (J–H) + 0.56$, we estimated the distance to the variable to be about $\sim$548 pc assuming $V_{\rm max} = 12.6$ (from the ASAS database). From Gazeas's (2009) three-dimensional correlations given below,

$$\begin{aligned}
\log M_1 &= 0.725(59)\log P - 0.076(32)\log q + 0.365(32)\\
\log M_2 &= 0.725(59)\log P + 0.924(33)\log q + 0.365(32)\\
\log R_1 &= 0.930(27)\log P - 0.141(14)\log q + 0.434(14)\\
\log R_2 &= 0.930(29)\log P + 0.287(15)\log q + 0.434(16)\\
\log L_1 &= 2.531(67)\log P - 0.512(51)\log q + 1.102(43)\\
\log L_2 &= 2.531(63)\log P + 0.352(52)\log q + 1.102(41),
\end{aligned}$$

the absolute parameters obtained using the value of q obtained from the cool spot solution are $M_1 = 1.22 \pm 0.12\ M_{\odot}$, $M_2 = 0.08 \pm 0.01\ M_{\odot}$, $R_1 = 1.34 \pm 0.05\ R_{\odot}$, $R_2 = 0.42 \pm 0.02\ R_{\odot}$, $L_1 = 2.66 \pm 0.48\ L_{\odot}$, and $L_2 = 0.25 \pm 0.03\ L_{\odot}$. Parameters obtained using the value of q from the hot spot solution lie within error bars. The derived values are a close match to those of SX Crv, which were spectroscopically deduced (Zola et al. 2004). They also lie within error bars of the values obtained for V1 from color indices and the derived mass ratio.

In conclusion, we report the period variation, photometric solution, and constancy of the Hα line of an overcontact binary ASAS J083241+2332.4. The O–C study suggests that a third body periodic variation of about 8.25 years is superimposed on the long-term period variation caused by mass transfer from the low mass to high mass component. Based on the photometric solution, V1 is an extremely low mass ratio system with a fill-out factor of $f\sim$ 50%–70%, and a high inclination of $i \sim 82°$. Only three other similar systems exist with such extremely low mass ratios: E53, V857 Her, and SX Crv. These systems along with V1 are very rare and challenge the existing theory that constrains the critical mass ratio to $\sim$0.07–0.09 based on various radiative and physical assumptions. Interestingly, V1 is identical in many astrophysical aspects to SX Crv as discussed above. We did not find any fill-in effect in the Hα line profile, suggesting that no significant activity is currently present in order to exhibit a strong O'Connell effect, though a trace of the O'Connell effect is seen in the present light curve. Even though V1 has a higher EW, it satisfies the correlation between period and intrinsic EW. We predict that as the activity increases, the correlation will strengthen. Although the O–C analysis strongly indicates the presence of a third body, we cannot entirely exclude the probable role of the Applegate mechanism. Further

observations are needed to confirm this result because our data show more scatter than the amplitude of the LITE variations. Moreover, continuous monitoring of this variable and similar new ones would enable us to decipher the degeneracy associated with the required critical mass ratio and the primary's mass, because, more or less, all of the theoretical models predict that systems with mass ratios similar to V1, and lower, do not exist because they eventually merge to form a fast rotating star over a timescale of 10^4–10^5 years (Rasio & Shapiro 1995).

We acknowledge the director of IUCAA, Pune and the director of IIA, Bengaluru for allocating time for the observations at IGO and HCT. We also thank Dr. Ranjan Gupta, IUCAA, for helping us with the observations. We thank the referee for valuable suggestions that led to the improvement of this paper. We thank Dr. Zasche for his valuable input regarding the code. K.S. acknowledges the support from UGC-BSR Research Start-up grant, Government of India. M.S. acknowledges the financial support from DST-SERB (Project No. SB/FTP/PS-184/2013) Government of India. Part of this work was performed at the Korea Astronomy and Space Science Institute, South Korea. The following internet based resources were used in this work: the NASA Astrophysics Data System, the SIMBAD database, and the VizieR service operated by CDS, Strasbourg, France, the ASAS, and the 2MASS databases.

REFERENCES

Applegate, J. H. 1992, ApJ, 385, 621
Applegate, J. H., & Patterson, J. 1987, ApJ, 322, 99
Arbutina, B. 2007, MNRAS, 377, 1635
Arbutina, B. 2009, MNRAS, 394, 501
Arbutina, B. 2012, POBeo, 91, 391
Barden, S. C. 1985, ApJ, 295, 162
Binnendijk, L. 1970, VA, 12, 217
Bonanos, A. Z. 2009, ApJ, 691, 407
Bradstreet, D. H., & Guinan, E. F. 1994, in ASP Conf. Ser. 56, Interacting Binary Stars, ed. A. W. Shafter (San Francisco, CA: ASP), 228
Cox, A. N. 2000, Allen's Astrophysical Quantities (4th ed.; New York: Springer)
Csizmadia, S., & Klagyivik, P. 2004, A&A, 426, 1001
Davidge, T. J., & Milone, E. F. 1984, ApJS, 55, 571
Drake, A. J., Djorgovski, S. G., Garcia-Alvarez, D., et al. 2014, ApJ, 790, 157
Eggleton, P. P., & Kisseleva-Eggleton, L. 2006, Ap&SS, 304, 75
Foukal, P. 1990, Solar Astrophysics, 492 (New York: Wiley-Interscience)
Frasca, A., Sanfilippo, D., & Catalano, S. 1996, A&A, 313, 532
Gazeas, K., & Stepien, K. 2008, MNRAS, 370, 29
Gazeas, K. D. 2009, CoAst, 159, 129
Gazeas, K. D., & Niarchos, P. G. 2006, MNRAS, 390, 1577
Gettel, S. J., Geske, M. T., & Mckay, T. A. 2006, AJ, 131, 621
Hilditch, R. W. 1989, SSRv, 50, 289
Hut, P. 1980, A&A, 92, 167
Irwin, J. B. 1959, AJ, 64, 149
Jiang, D., Han, Z., Wang, J., Jiang, T., & Li, L. 2010, MNRAS, 405, 2485
Kaluzny, J., Thompson, I. B., Rozyczka, M., & Krzeminski, W. 2013, AcA, 63, 181
Kandulapati, S., Devarapalli, S. P., & Pasagada, V. R. 2015, MNRAS, 446, 510
Kaszas, G., Vinko, J., Szatmary, K., et al. 1998, A&A, 331, 231
Kiron, Y. R., Sriram, K., & Vivekananda Rao, P. 2011, RAA, 11, 1067
Kiron, Y. R., Sriram, K., & Vivekananda Rao, P. 2012, BASI, 40, 51
Kwee, K. K., & van Woerden, H. 1956, BAN, 12, 327
Lanza, A. F., & Rodono, M. 2002, AN, 323, 424
Lenz, P., & Breger, M. 2005, CoAst, 144, 41
Li, L., & Zhang, F. 2006, MNRAS, 369, 2001
Linsky, J. L., Bornmann, P. L., Carpenter, K. G., et al. 1982, ApJ, 260, 670
Lucy, L. B. 1967, ZA, 65, 89
Maceroni, C., Montalban, J., Michel, E., et al. 2009, A&A, 508, 1375
Mateo, M., Harris, H. C., Nemec, J., & Olszewski, E. W. 1990, AJ, 100, 469
Milone, E. F. 1969, CoKon, 65, 457
Mochnacki, S. W. 1981, ApJ, 245, 650
Mochnacki, S. W., & Doughty, N. A. 1972, MNRAS, 156, 243
Nandez, J. L. A., Ivanova, N., & Lombardi, J. C., Jr. 2014, ApJ, 786, 39
Nefs, S. V., Birkby, J. L., Snellen, I. A. G., et al. 2012, MNRAS, 425, 950
O'Connell, D. J. K. 1951, PRCO, 2, 85
Pepper, J., Stanek, K. Z., Pogge, R. W., et al. 2008, AJ, 135, 907
Pribulla, T., Chochol, D., Rovithis-Livaniou, H., & Rovithis, P. 1999, A&A, 345, 137
Pribulla, T., & Rucinski, S. M. 2006, AJ, 131, 2986
Pribulla, T., & Rucinski, S. M. 2008, MNRAS, 386, 377
Prsa, A., & Zwitter, T. 2005, ApJ, 628, 426
Qian, S. B., Yang, Y., Zhu, L., He, J., & Yuan, J. 2006, ApSS, 304, 25
Qian, S.-B., Zhu, L.-Y., Soonthornthum, B., et al. 2005, AJ, 130, 1206
Rasio, F. A., & Shapiro, S. L. 1995, ApJ, 438, 887
Reid, I. N., & Hawley, S. L. 2005, Springer-Praxis books in Astrophysics and Astronomy (Berlin: Springer)
Rucinski, S. M. 1969, AcA, 19, 245
Rucinski, S. M. 1992, AJ, 103, 960
Rucinski, S. M. 1994, AJ, 107, 738
Rucinski, S. M., Lu, W., Mochnacki, S. W., Ogloza, W., & Stachowski, G. 2001, AJ, 122, 1974
Rucinski, S. M., Pribulla, T., & Budaj, J. 2013, AJ, 146, 70
Sriram, K., Kiron, Y. R., & Vivekananda Rao, P. 2009, RAA, 9, 1149
Stauffer, J. R., & Hartmann, L. W. 1986, Cool Stars Stellar Systems and the Sun (Berlin: Springer)
Stepien, K. 2006, AcA, 56, 199
Stepien, K. 2011, AcA, 61, 139
Stepien, K. 2012, A&A, 531, A18
Szalai, T., Kiss, L. L., Meszaros, Sz., Vinko, J., & Csizmadia, Sz. 2007, A&A, 465, 943
Terrell, D., & Wilson, R. E. 2005, ApSS, 296, 221
Tylenda, R., Hajduk, M., Kaminski, T., et al. 2011, A&A, 528, A114
Van Hamme, W. 1993, AJ, 106, 209
Van Hamme, W., & Wilson, R. E. 2003, in ASP Conf. Ser. 298, Gaia Spectroscopy: Science and Technology, ed. U. Munari (San Francisco, CA: ASP), 323
Vilhu, O., & Maceroni, C. 2007, in IAU Symp. 240, Binary Stars as Critical Tools & Tests in Contemporary Astrophysics, ed. W. I. Hartkopf, E. F. Guinan, & P. Harmanec (Cambridge: Cambridge Univ. Press), 719
Vilhu, O., & Rusinski, S. M. 1983, A&A, 127, 5
Vilhu, O., & Walter, F. M. 1987, ApJ, 321, 958
Webbink, R. F. 1976, ApJ, 209, 829
Webbink, R. F. 2003, in ASP Conf. Ser. 293, 3D Stellar Evolution Contact Binaries, ed. S. Turcotte et al. (San Francisco, CA: ASP), 76
Wilson, R. E. 1979, ApJ, 234, 1054
Wilson, R. E. 1990, ApJ, 356, 613
Wilson, R. E. 2006, in ASP Conf. Ser. 349, Astrophysics of Variable Stars, ed. C. Sterken & C. Aerts (San Francisco, CA: ASP), 71
Wilson, R. E., & Devinney, E. J. 1971, ApJ, 166, 605
Woltjer, J., Jr. 1922, BAN, 1, 93
Young, A., Skumanich, A., & Harlan, E. 1984, ApJ, 282, 683
Zasche, P., Liakos, A., Niarchos, P., et al. 2009, NewA, 14, 121
Zola, S., Rucinski, S. M., Baran, A., et al. 2004, AcA, 54, 299